Central peak in the pseudogap of high T_c superconductors

D. K. Sunko and S. Barišić

Department of Physics, Faculty of Science, University of Zagreb, POB 331, HR-10000 Zagreb, Croatia.

ABSTRACT

A detailed theoretical description is provided of the narrow low-energy peak in the ARPES response of superconducting optimally doped and weakly underdoped BSCCO near the van Hove point. The pseudogap is taken to be due to electron-paramagnon scattering. The narrow peak is antiadiabatic: it consists of electrons which are so slow that the scattering is not effective in suppressing their spectral strength. We find two temperature regimes for the pseudogap. The low-temperature one is relevant for experiment in BSCCO, where the paramagnon band-edge is much higher than the temperature. The high-temperature regime occurs when the band-edge is lower than the temperature. It is characterized by hot spots when the band-edge is finite, and develops a macroscopic antiferromagnetic potential when it vanishes. We argue that it is relevant for the electron-doped high-T_c compounds. Our work gives a connection between the simultaneous appearance of a magnetic resonance and a narrow low-energy feature in ARPES at the superconducting transition in BSCCO. In the model, both can be obtained by switching the paramagnon damping from supercritical to subcritical, without even including the superconducting correlations explicitly. The leading edge scale of the narrow peak is controlled by the chemical potential and is incidental to the pseudogap mechanism, whose physical scale is given by the high-energy 'hump.'

Keywords: ARPES, pseudogap, high-T_c, superconductivity

1. INTRODUCTION

The rich phenomenology of high-T_c materials is only matched by the variety of theoretical attempts to explain it. A dominant and unifying point of view, capable of ordering the phenomena with respect to importance or simplicity, is still lacking. Once experiment moves away from the macroscopic thermodynamic manifestations, which are generically not sensitive to the microscopic mechanism, one is faced with the fact that doped copper oxide perovskites are far more complex than metals. Careful comparative studies, with an end to establish what is typical across a broad class of these materials, and what is more immediately connected with the superconducting ones, have yet to run their course.

The present work is based on two theoretical premises. First, it is possible to order the relevant physical scales in a well-resolved hierarchy, in which each level is primarily responsible for one aspect of the observations. Second, it is desirable at low temperature to separate the effects of superconductivity proper from those inherited from the 'strange metal' in which it occurs. We concentrate on the vicinity of optimal doping, and do not feel constrained to account simultaneously for the particular mechanism of the metal-insulator transition at half-filling. Instead we incorporate the correlations responsible for it within a slave boson framework, starting from the metallic limit.

Within the above broad theoretical framework, we focus our attention on a particular long-standing issue. The ARPES signal in the $Bi_2Sr_2CaCu_2O_8$ class of compounds (BSCCO) near the van Hove point is represented by one of the most extensive body of data of any high-T_c material or technique.[1–10] Its most prominent feature at optimal doping is the 'peak-dip-hump' profile, with a narrow low-energy peak superimposed on a broad maximum at higher energy. The peak disappears with underdoping, revealing the well-known pseudogap form, due to the surviving high-energy structure.

The gist of our proposed interpretation is as follows. The highest energy scale, large on-site Coulomb repulsion, is responsible for a renormalization of the band parameters. A physical foundation for this renormalization is laid by explicitly including the oxygen degree of freedom in our approach. Once the stage is set, the next scale is that of dispersive paramagnons, giving rise to the pseudogap structure characterized by the high-energy hump. However, the pseudogap is not equally efficient in suppressing all electrons. Near the vH point some are so slow that they do not scatter off the paramagnons, and survive as a narrow 'antiadiabatic' peak in the middle of the pseudogap. The binding energy of this

Email: dks@phy.hr, sbarisic@phy.hr

peak, a few hundred Kelvin, is alredy competitive with the superconducting scale, but in fact has no dynamical scale of its own. Instead it is primarily determined by the chemical potential.

Our work relates the simultaneous appearance of a magnetic resonance[11,12] and narrow ARPES peak when BSCCO becomes superconducting. In the model, both are achieved by switching the paramagnon damping from supercritical (above T_c) to subcritical (below T_c). Thus we are able to account for the superconducting ARPES profile without explicit treatmet of superconducting correlations. However, the superconducting (pseudo)gap is not included in the present analysis.

An unexpected side benefit of the above systematic approach is that it provides an insight into the strong 'hot-spot' suppression of the ARPES signal in electron-doped materials, such as $Nd_{1.85}Ce_{0.15}CuO_4$ (NCCO), which was never observed in the hole-doped ones. Namely, we find two regimes in our calculation, according to whether the temperature is higher or lower than the paramagnon band-edge. In BSCCO, the latter is the case, and the resulting 'low-temperature' or 'quantum' pseudogap has no hot-spot effect. In NCCO, on the other hand, superconductivity coexists with AF correlations of a characteristic energy lower than superconductivity.[13,14] In our model, such a 'high-temperature' or 'semiclassical' pseudogap is strongly affected by the hot-spot effect.

In the literature, a number of different scenarios have been put forward to account for the peak-dip-hump structure. Bilayer splitting[6,15,16] is completely different from our proposal; in it the high-energy hump is ascribed to another band. Phonons[17–20] with a strong (π,π) response cannot be excluded in principle by our calculation, since the boson in question is modelled quite generically and from the side of unbroken symmetry. However, we find it more natural to think in terms of the observed paramagnons.[21] Stripes[22] could be added to our calculation in the form of a weakly dispersive low-energy 'central peak' in the magnon response. They could play a role in the shape of the final ARPES profile, however we establish the main scales and dispersions in substantial agreement with experiment already without them. In contrast to the calculation of Eschrig and Norman,[23] which fits the Fermi surface precisely already at the level of an effective band dispersion, with several non-nearest neighbor hoppings, we fit the main FS features with a three-band nearest-neighbor dispersion renormalized by strong Coulomb effects, and correct the shape near the vH points by much weaker magnetic effects. Also, instead of considering superconductivity and magnetism simultaneously in the symmetry-broken state,[23] we proceed from the side of unbroken symmetry, and take superconductivity into account only indirectly, through the observed low-temperature paramagnon response, as outlined above. Conversely, Vilk[24] has used a calculation similar to ours to account for shadow bands. We also find a regime in which the narrow peak follows a shadow-band dispersion, but it does not give the systematics of the peak-dip-hump feature described here.

2. THEORETICAL FRAMEWORK

2.1. Strong Coulomb repulsion

The strong on-site repulsion of holes sharing a common copper d-orbital provides the highest scale in the problem, usually estimated at more than 5 eV. As in other metal oxides, it is generally agreed to be responsible for the insulating state at half-filling,[25] however the evolution of this state with doping through the so-called pseudogap regime towards the optimally doped state has been the subject of varying interpretations. The differentiating question is whether a model for the optimally doped state should at the same time be capable of describing the metal-insulator transition at low doping. An affirmative answer is reflected in the use of one-band models of t–J type in the whole doping range,[26] typically with more than one hopping integral when one wishes to account for the phenomenology near optimal doping.[23]

Conversely, one may feel free to describe the optimally doped state as essentially metallic, with the local repulsion reflected in a strong renormalization of the band parameters relative to the prediction of chemical calculations. The slave boson approach has become characteristic of this attitude,[27] which is in the background of our calculation as well.

A systematic slave boson study[28] of the three-band Emery model[29] has established a range of effective parameters which do reflect a significant renormalization of the bare ones, due to strong on-site repulsion on the coppers. The salient point is that when the direct oxygen-oxygen hopping is taken into account, the calculation allows a renormalized regime in which the effective copper-oxygen overlap is much less than the oxygen-oxygen one, despite the initial (bare) overlaps having been in the opposite limit. This zeroth-order effect on the band parameters is all that remains of the on-site repulsion in our approach. The effective open band in the model is

$$\varepsilon(\mathbf{k}) = \frac{1}{3}\sqrt{P}\left(\cos\frac{\Psi}{3} + \sqrt{3}\sin\frac{\Psi}{3}\right), \tag{1}$$

where

$$\begin{aligned}\Psi &= \arccos\frac{Q}{P^{3/2}},\\ P &= 12t^2 f_1 + 48t'^2 f_2 + \Delta_{pf}^2,\\ Q &= 144t'(3t^2 + t'\Delta_{pf})f_2 - \Delta_{pf}(18t^2 f_1 + \Delta_{pf}^2),\end{aligned}$$

with $f_1 = \sin^2 k_x/2 + \sin^2 k_y/2$ and $f_2 = \sin^2 k_x/2 \sin^2 k_y/2$. Here all parameters refer to the final renormalized values: copper-oxygen splitting $\Delta_{pf} = 3.6$ eV, copper-oxygen overlap $t = 0.3$ eV, and oxygen-oxygen overlap $t' = -1$ eV. In contrast to one-band models, they enter non-linearly into the expression for the band dispersion. This is reminiscent of the situation in LDA calculations, where the projection of a multiband model onto an effective single band similarly gives rise to non-linear dependence on the initial parameters.[30] We emphasize that while the quoted numerical values have been chosen to fit experiment, they do fall into the range characteristic of strong renormalization, as found by the slave boson studies.[28] In particular, the ratio $\Delta_{pf} \approx -4t'$ turns out to be characteristic of the strong-coupling limit.

In the present work, the connection between the above strong-coupling framework and the magnetic perturbations is phenomenological. In a fully consistent slave boson picture, the magnetic part comes from fast fluctuations in the spin channel, as opposed to the slow fluctuations in the charge channel, which give rise to the effective band renormalizations, described above. Such a complete theory is currently under development.

2.2. Weak magnetic perturbation

Magnetic phenomena have been extensively studied in the high-T_c superconductors, which after all are oxides, sooner expected to be antiferromagnetic than superconducting.[11, 12, 31–39] In superconducting BSCCO, there is a distinct magnetic resonance of uncertain microscopic origin,[12, 34, 36] appearing at 41 meV simultaneously with superconductivity, and corresponding to a correlation length of 2–3 lattice spacings. Morr[40] has shown in a simple model calculation that its connection with superconductivity need not be any deeper than through a sudden reduction in paramagnon damping, which we may associate plausibly enough with the opening of the superconducting gap. We describe the resonance by the same (simplest possible) model, with dispersive branches out of a commensurate minimum:

$$\omega_D(\mathbf{Q}+\mathbf{q})^2 = \widetilde{\omega}^2 + c^2|\mathbf{q}|^2, \tag{2}$$

where $\mathbf{Q} = (\pi, \pi)$ is the AF wave vector, $\widetilde{\omega}$ is the paramagnon band-edge, and c their velocity. The paramagnon propagator is similarly taken as simple as possible,

$$\chi_R(\mathbf{Q}+\mathbf{q},\omega) = \frac{\omega_0^2}{(\omega+i\gamma)^2 - \omega_D(\mathbf{Q}+\mathbf{q})^2}, \tag{3}$$

where γ is the damping, and ω_0 some cutoff frequency, corresponding to the extension $\xi_0 = c/\omega_0$ of the paramagnon anomaly around $\mathbf{Q}$. The relationships of the various parameters are shown in Fig. 1.

The band-edge $\widetilde{\omega}$ determines the physical regime both with respect to the damping and to the temperature, as discussed below. We do not take into account possible slow, low energy correlations such as incommensurate stripes. That would require an explicit modelling of a central peak in the magnon response $\mathrm{Im}\,\chi$. While it cannot be excluded at present that stripes have some role in shaping the observed ARPES profile, it is one result of the present work that as far as the principal physical scales and dispersions near the vH point are concerned, one can do without them.

2.3. Perturbative regimes

The paramagnon perturbation is taken into account by the basic one-loop contribution of Fig. 2. We neglect vertex corrections. It has been noticed that in the absence of Migdal's theorem, vertex corrections tend to cancel with those from self-consistency,[41, 42] so it seems more reliable to use the free (non-self-consistent) fermion propagator at the same time. The usual expression for the retarded self-energy[43] may be profitably rewritten as

$$\begin{aligned}\Sigma_R(\mathbf{k},\omega) = -\frac{1}{2\pi^2}\int g^2_{\mathbf{k},\mathbf{q}} d^2q \int_{-\infty}^{\infty} d\omega' \quad \Big[&\chi_R(\mathbf{Q}+\mathbf{q},\omega-\omega')(1-f(\omega'))\mathrm{Im}\,G_R^{(0)}(\mathbf{k}-\mathbf{q}-\mathbf{Q},\omega')\\ &+G_R^{(0)}(\mathbf{k}-\mathbf{q}-\mathbf{Q},\omega-\omega')n(\omega')\mathrm{Im}\,\chi_R(\mathbf{Q}+\mathbf{q},\omega')\Big],\end{aligned} \tag{4}$$

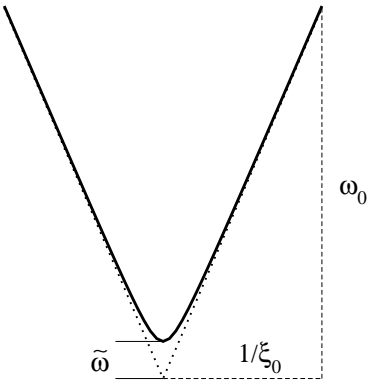

Figure 1. Parametrization of the paramagnon dispersion. The slope is the velocity $c = \xi_0 \omega_0$.

where $g_{\mathbf{k},\mathbf{q}}$ is the effective interaction vertex in Fig. 2. The free electron propagator is just

$$G_R^{(0)}(\mathbf{k},\omega) = \frac{A_{\mathbf{k}}}{\omega - \varepsilon(\mathbf{k}) + \mu + i\eta}, \tag{5}$$

with $\varepsilon(\mathbf{k})$ from Eq. (1), and $A_{\mathbf{k}}$ the spectral density of the resonant band. We shall eventually absorb it into a coupling constant, $F \equiv g^2_{\mathbf{k},\mathbf{q}} A_{\mathbf{k}}$. This limits our calculation to a qualitative one away from the vH point, since we expect a significant variation in $A_{\mathbf{k}}$ along the Fermi surface, based on the above slave boson considerations. The two terms contributing to Σ have a transparent physical interpretation: the first is the paramagnon propagator convoluted with the electron response, the second, vice versa.

There are three physical guidelines to our calculation, and two can be discerned already in Eq. (4). First, if the paramagnon response is peaked around $\mathbf{Q} = (\pi, \pi)$, the main contribution to Σ at $\mathbf{k} \approx (\pi, 0)$, the vH point, comes from electrons at $\mathbf{k} - \mathbf{Q} \approx (0, -\pi)$, the other vH point, where they are slow. Hence the antiadiabatic electrons form, as it were, a subsystem of their own, and avoid the pseudogap suppression of the spectral strength, affecting the fast electrons as they scatter adiabatically off the slow magnons.

Second, the two terms have very different contributions to the self-energy depending on whether the temperature is higher or lower than the paramagnon band-edge. When $kT \gg \widetilde{\omega}$, the second (boson-response) term dominates, simply because there are many bosons, $n(\omega') \to kT/\omega_D(\mathbf{Q}+\mathbf{q}) \approx kT/\widetilde{\omega} \gg 1$, which is the classical limit. The bosons are near condensation, and about to build up a macroscopic AF potential, leading to the halving of the zone. In this high-temperature limit, the pseudogap evolves towards the true gap as $\widetilde{\omega}/kT \to 0$.

In the low-temperature limit, $kT \ll \widetilde{\omega}$, there are only quantum zero-point fluctuations of the paramagnons, and the two terms are competitive. Their dynamics is somewhat different than in the high-temperature case, where the semiclassical limit of the boson number effectively induces an additional dispersive term $\omega_D(\mathbf{Q}+\mathbf{q})$ in the denominator. In this low-temperature limit, the pseudogap becomes practically independent of temperature, as long as the band-edge is kept fixed.

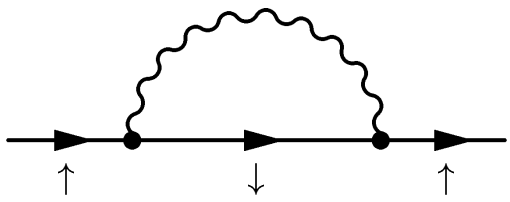

Figure 2. One-loop contribution to the self-energy. The fermion propagator is free, and there are no vertex corrections.

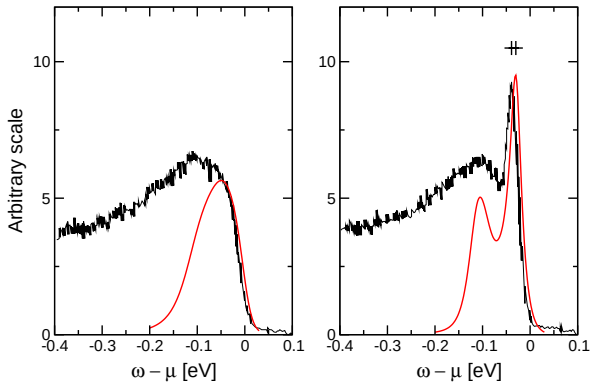

Figure 3. Comparison with experiment[3] on BSCCO (jagged line), left: T=103 K, right: T=46 K. Calculation (smooth curves), left: overdamped magnons, right: underdamped magnons (parameters in the text). The chemical potential is $\mu = 0.025$ eV away from the vH point. The vertical scales of the two experimental and the two theoretical curves are the same, while the relative scale of theory vs. experiment is arbitrary.

The third point relevant to establish a physical regime is less immediately obvious. The antiadiabatic central peak in the electron response is sensitive to the paramagnon damping γ. It appears only in the underdamped limit, $\gamma < \widetilde{\omega}$. In the opposite limit, only a diffusive pseudogap survives in principle, although a wide and low remnant of the central peak can also be seen if the damping is not too large. It is noteworthy that the damping of the antiadiabatic peak is directly related to the paramagnon damping. The consequence is that even in the underdamped regime, $\mathrm{Im}\,\Sigma$ can be different from zero even though the peak is at the Fermi energy, $\mathrm{Re}\,\Sigma = 0$. This very simple device to violate the Fermi liquid paradigm only depends on the fact that the boson damping has a fixed constant value.

3. PARAMETRIZATION AND TEMPERATURE REGIME

In Fig. 3, we show the comparison with experiment, used to establish the parametrization. The jagged lines are measured ARPES intensities[3] of optimally doped BSCCO, integrated along the $(0,0)$–$(\pi,0)$ line, in the normal (T=103 K, left) and superconducting state (T=46 K, right). The smooth lines are both calculated at the $(\pi,0)$ point, the only difference being the paramagnon damping: left, overdamped ($\gamma = 0.06$ eV), right, underdamped ($\gamma = 0.015$ eV). The other parameters are: the band-edge $\widetilde{\omega} = 0.04$ eV, cutoff $\omega_0 = 0.15$ eV, and correlation length $\xi = c/\widetilde{\omega} \sim$3 lattice spacings. The coupling constant is $g^2_{\mathbf{k},\mathbf{q}} A_{\mathbf{k}} \equiv F = 0.077$ eV. Relative to the particular parametrization of the effective band (1), this amounts to about 10% of the electron bandwidth, as renormalized by the strong on-site repulsion.

The central peak does not straddle the Fermi energy. Generically, its position is determined by the chemical potential. In addition, it has its own dispersion, albeit quite flat in the vicinity of the vH point. It is of course well known that the narrow feature in BSCCO does not appear at the Fermi energy, however since it is correlated with superconductivity, it is easy to ascribe the discrepancy to the superconducting gap. In fact, part of the observed binding energy of the narrow peak may be an intrinsic pseudogap property, as obvious from the figure.

In Fig. 4, we show how the correction to the effective band Fermi surface, due to the paramagnon interactions, selects the correct temperature regime for the calculation. When the peak does not cross the Fermi energy, an accepted alternative definition[7] of the Fermi surface is the locus of maxima in the momentum distribution curves (MDC), which is just the spectral strength at $\omega = \mu$, $A(\mathbf{k}, \omega = \mu)$.

The initial Fermi surface of the band (1) is shown as a thin line. It is too steep relative to experiment near the vH point. Including the paramagnon self-energy effects leads to qualitatively different outcomes (thick lines) according to the temperature regime. At left is the prediction of the high-temperature regime, $kT \gg \widetilde{\omega}$. There is a clear tendency of the Fermi surface to bend towards the new zone boundary (dashed line), where the gap opens when $\widetilde{\omega}/kT \to 0$. At right, the low-temperature prediction is just the opposite, the Fermi surface bends away from the diagonal, even curving slightly upwards in our calculation. Since the observed BSCCO Fermi surface is of the latter type, we choose the low-temperature regime as the one relevant for experiment in our model.

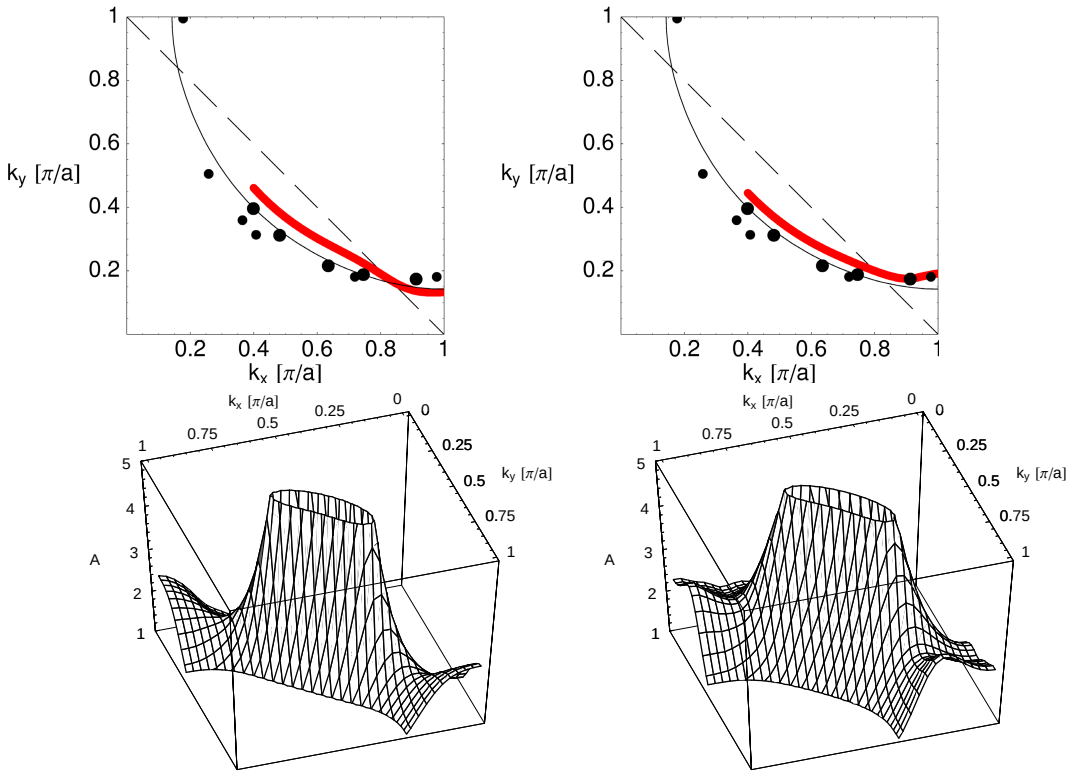

Figure 4. Fermi surfaces (top row) and renormalized spectral functions $A(\mathbf{k}, \omega = \mu)$ (bottom row). Left column: high-temperature limit, $kT = 0.1$ eV and $F = 0.2$ eV. In the 3D plots the paramagnon band-edge is lowered to 0.01 eV to make the saddles more easily visible. Points: experimental FS crossings, large: Ref. 44, small: Ref. 45. Here $\mu = 0.015$ eV.

The theoretical insight is that hot-spot effects[46] are to be expected only in the high-temperature regime. In fact they have never been observed in ARPES on BSCCO, a puzzle solved in the model by choosing the opposite regime. The difference between the spectral strengths $A(\mathbf{k}, \omega = \mu)$ is shown in the lower row of Fig. 4, calculated with a somewhat lower band-edge, to exaggerate the effect visually. The hot-spot is visible as a saddle on the left (high-temperature) plot. The low-temperature plot at right also has a saddle, but it is away from the diagonal. The symmetry-based prediction of the intensity dip on the skew-diagonal $(\pi, 0)$–$(0, \pi)$ (hot-spot effect) is only borne out for the boson-response term, which dominates in the classical limit. This is visible from the structure of Eq. (4), in which the second term alone is responsible for the eventual classical AF potential, which halves the zone.

4. COMPARISON WITH EXPERIMENT

4.1. The case of BSCCO

In Fig. 5, we show a detailed comparison with another experiment for the parametrization given in the previous section. Since that was fixed at the $(\pi, 0)$ point alone, Fig. 5 is a parameterless prediction of the model for the evolution of the ARPES signal in the Brillouin zone along the $(\pi, 0)$–(π, π) line and parallel to it. All the qualitative experimental features are correctly obtained: both the major and minor energy scales, and the downturn (in energy) of the antiadiabatic peak as one moves further away from the Fermi crossing. Such an approaching-then-receding of the narrow peak with respect to the Fermi level has been noticed in experiment,[7] and becomes more pronounced with underdoping.

In the right two panels of Fig. 5, we show what happens as one moves towards the Γ point in cuts parallel to the X–M line. We note a significant redistribution of spectral strength, such that the side peak is much stronger at $k_y = 0$, the Γ–X line itself, but quickly loses strength as one moves perpendicularly away from it in the k_y direction, parallel to the X–M line. Finally at $k_y = 0.35\pi/a$, only the antiadiabatic peak survives. Experimentally, much the same behavior has

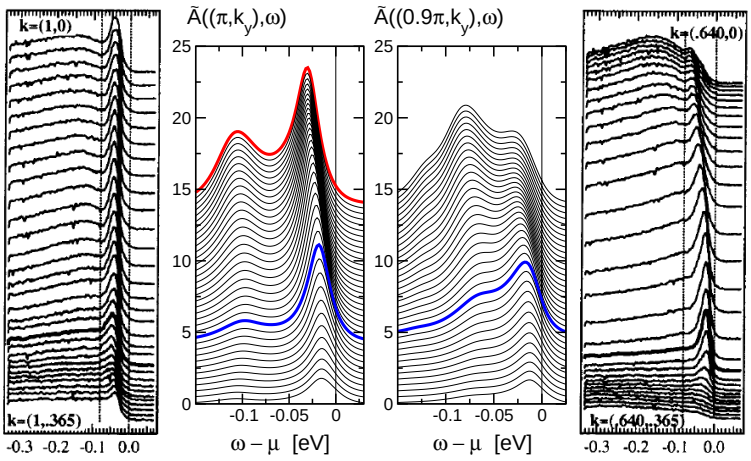

Figure 5. Left to right: a) experimental EDC's along the X–M line, from $k_y = 0$ (top) to $k_y = 0.365\pi$ (bottom), multiplied by a Fermi function at 100 K and offset for clarity.[7] b) Calculated intensities for the same situation. c) the same for the line parallel to X–M at $k_x = 0.9\pi$. d) experiment for the line parallel to X–M at $k_x = 0.64\pi$. EDC's corresponding to the Fermi surface crossing from the maximum in the momentum distribution curve are given by a thicker line. Here $\mu = 0.025$ eV.

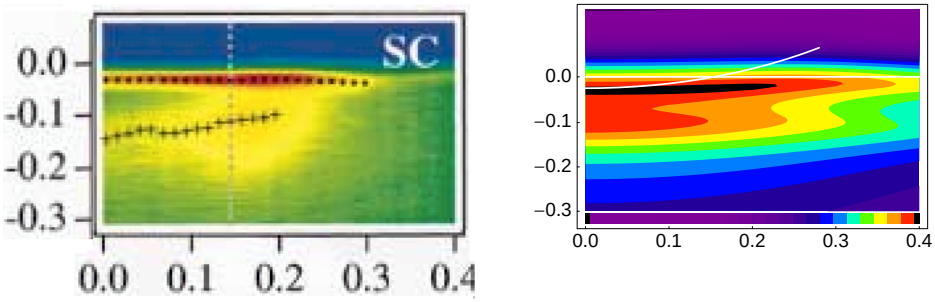

Figure 6. Experimental[7] log-intensity distribution in optimally doped BSCCO (left), compared with the present calculation (right). The vertical scale is in eV from the Fermi energy, the horizontal one in π/a along the $\pi, 0$–π, π line. White lines: horizontal, Fermi energy; curved, unperturbed $U_d = \infty$ dispersion. The intensities are multiplied by a Fermi factor at 100 K.

been observed, with the proviso that it seems to evolve more slowly in the Γ direction, so the qualitative picture we obtain around $k_x = 0.9\pi$ in the calculation is observed around $k_x = 0.64\pi$ in experiment.[7] Again, the wide peak has its own approaching-then-receding sequence, similar to the one observed both in optimally doped[7] and underdoped samples.[47] The fact that the calculated qualitative features continue to match closely the experimental situation as one moves away from the X–M line into the zone interior, while the quantitative evolution proceeds at a different pace, is possibly due to neglecting the **k**-dependence of the product $g^2_{\mathbf{k},\mathbf{q}} A_{\mathbf{k}}$ in the calculation.

Figure 5 gives an independent indication that the low-temperature regime is observed in BSCCO. It is not difficult to get similar scales in the high-temperature regime. However, the evolution of the strength distribution between the narrow and wide peaks is qualitatively different. In the high-temperature calculation, the narrow peak disappears sooner as one moves away perpendicularly from the $(0, 0)$–$(\pi, 0)$ line. As visible in the figure, the opposite happens in experiment, and only the narrow peak survives. This is also found in the low-temperature calculation, so both the Fermi surface correction and the spectral strength redistribution indicate that the pseudogap in BSCCO is due to quantum zero-point fluctuations.

Figure 6 shows an intensity plot of the same calculation as in the left panels of Fig. 5, compared with the same experiment.[7] The narrow 'tongue' of the low-energy feature can be clearly discerned. It has a much flatter dispersion than the original renormalized band (1). There are two ways in which it can revert to it: reducing the coupling constant, and increasing the paramagnon band-edge. The first sounds trivial, but if the band-edge is simultaneously low, the system

behaves all the time as if it were in a strong-coupling limit: the narrow peak persistently follows a shadow-band dispersion, no matter how small the coupling constant is. (A similar regime was studied by Vilk.[24]) The weak-coupling limit is finally recovered through the reduction of the pseudogap splitting, the side wings finally closing in on the antiadiabatic peak. Increasing the band-edge, on the other hand, gives rise to the predictable outcome: the side wings lose strength, and the central peak takes on the characteristics of a weakly affected quasiparticle, following the original band dispersion.

4.2. The case of NCCO

Electron-doped cuprates should *a priori* be in a completely different physical regime than the hole-doped ones. In particular, one would expect[28] that the slave boson mean-field renormalization of Δ_{pf} due to large on-site repulsion is not strong even at zero doping. In a model calculation which contained no oxygen-oxygen hopping, this was found to be the case.[48] It suggests the 'bare' copper-oxygen splitting $\Delta_{pd} \approx \Delta_{pf}$, hence $\Delta_{pf} \gg t, |t'|$ in the notation of Eq. (1). The other natural assumption $t > |t'|$ is difficult to reconcile with the ARPES data[49–54] in $Nd_{1.85}Ce_{0.15}CuO_4$, whose Fermi surface is both of nearly circular shape and crosses the skew-diagonal of the zone. Such a shape is qualitatively different than expected in the above case; whenever the band is dominated by the Cu–O hopping t, the Fermi surface in the vicinity of the skew-diagonal tends to be parallel with it, especially near the point $(\pi/2, \pi/2)$.

Interestingly enough, we can easily reproduce the shape of the Fermi surface in NCCO in a regime very similar to the one used for BSCCO, namely $\Delta_{pf} > -t' \gg t$, the main difference being that Δ_{pf} is now significantly smaller than $4|t'|$: $\Delta_{pf} = 1.6$ eV, $t' = -1.2$ eV and $t = 0.3$ eV. We emphasize that these values are found simply as 'best-fit' parameters for the Fermi surface. Nevertheless, it is noteworthy that the zeroth-order band prediction indicates that the effect of the oxygen hopping channel is as large in the electron-doped cuprates as in the hole-doped ones. From the slave boson studies cited above, we recognize this parameter regime as one which does not reflect a significant renormalization of Δ_{pf} at the slave boson mean-field level.

The ARPES spectra of NCCO show a strong hot-spot effect. In Fig. 7 we use a schematic choice of parameters to test our previous understanding, that this is a mark of the high-temperature regime. In the left panel, the temperature is $kT = 0.1$ eV. For numerical reasons, the paramagnon band-edge is taken not too low, $\widetilde{\omega} = 0.01$ eV, and the damping is raised to $\gamma = 0.02$ eV, so we are in the overdamped regime. The other parameters are as in the BSCCO fit, except that $F = 0.13$ eV. For the low-temperature regime, we put $kT = 0.005$, half the band-edge. In order to make a fair comparison, one has to increase the coupling constant, since in the high-temperature case it benefited from an effective factor $kT/\widetilde{\omega}$, the (diverging) boson occupation. We put $F = 0.77$ eV, in order that the pseudogap splitting of the ARPES profile at the hot-spot position be the same as in the low-temperature case. This *forces* the appearance of a hot-spot effect in the low-temperature case as well, providing the most stringent test of the regime choice.

There is a clear difference between the two regimes in Fig. 7. In the high-temperature case (left), the hot-spot is strongly dipped relative to the maximum on the diagonal. At low temperature (right), there is also a minimum at the hot spot, but it has been bought at the price of a considerable attenuation of the whole ridge parallel to the skew-diagonal, so the relative attenuation is much smaller. In addition, the 'horns' in the momentum distribution surface near the edge of the zone have merged into a continuous high ridge.

The comparison with experiment in Fig. 8 gives grounds to choose the high-temperature regime. The measured relative suppression at the hot-spot seems rather strong, and the minimum fairly well defined, although we cannot say how much, because the published figure contains no color scale. In addition, near the edge of the zone there are several distinct maxima, just as in our high-temperature plot. We can even obtain two maxima in the ridge on the diagonal, simply by increasing the damping to $\gamma = 0.03$ eV, but at the cost of a loss of intensity at the edge of the zone. A more detailed study of these and other effects is under way.

While the above schematic calculation cannot be regarded as definitive, it establishes two qualitative points: the relevance of the oxygen hopping for NCCO, and that whatever magnetic mode is responsible for the hot spots in ARPES should be at lower energy than the superconductivity. Since measurements are made below $T_c \approx 20$ K, the implication is that there are magnetic correlations with energy near zero. This is in accord with the broad phase diagram of the electron-doped cuprates, where the SC and AF phases lie next to each other, unlike the hole-doped situation where they are separated by the pseudogap phase. The overdamped limit also fits in with the absence of a strong narrow feature in the ARPES profiles of NCCO.

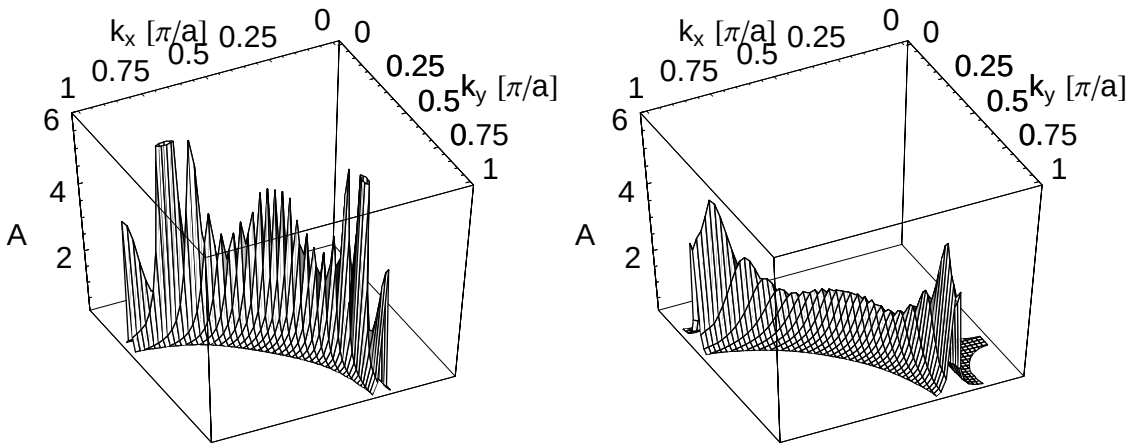

Figure 7. Spectral strength $A(\mathbf{k}, \omega = \mu)$ calculated for $Nd_{1.85}Ce_{0.15}CuO_4$, in the high-temperature (left) and low-temperature (right) limits. Hot spot attenuation is clearly visible as a saddle where the FS intersects with the diagonal. The chemical potential is $\mu = 0.75$ eV, corresponding to 9% electron doping.

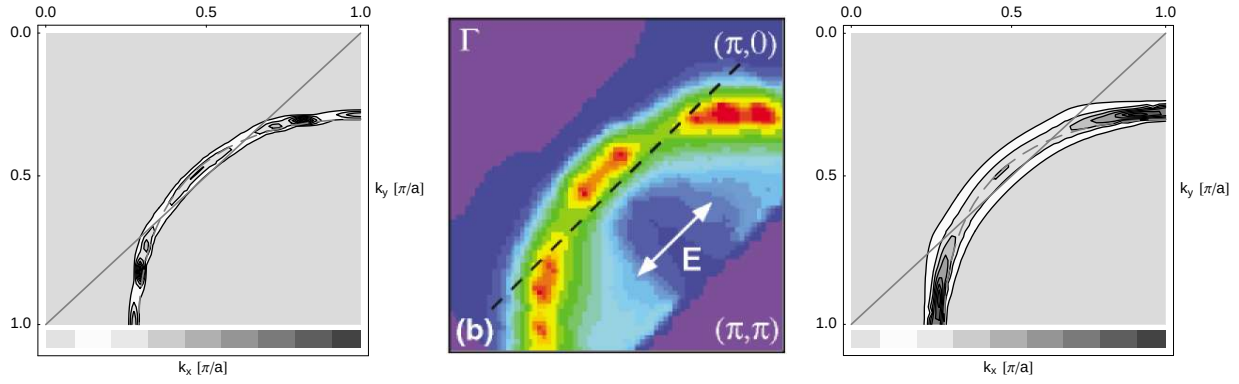

Figure 8. Experimental ARPES spectra[51] of $Nd_{1.85}Ce_{0.15}CuO_4$ (middle, unknown color scale). Left and right are contour plots of the 3D surfaces in Fig. 7, both drawn to the gray scale of the left one. The dashed lines in the latter contour plots give the zeroth-order FS for the dispersion (1).

5. CONCLUSIONS

The main physical result of this work is that the pseudogap in optimally doped BSCCO is in fact fully developed, and of the order of 1000 K. The narrow low-energy feature which makes it appear otherwise is an antiadiabatic peak in the middle of the pseudogap, which is part of the same dynamical picture. In particular, its binding energy is essentially determined by the chemical potential, not by any separate phenomenon.

In our model, the pseudogap in BSCCO is due to zero-point motion of the magnons, whose characteristic energy is of the order of 400 K, much higher than the superconducting transition. Such a 'low-temperature' pseudogap does not require any additional ground-state phenomena (except superconductivity), simply because it is already effectively at zero temperature. One would of course like to understand why the magnetic correlations undergo an essential change at T_c. We believe that within our theoretical framework, such questions can be treated by a complete slave boson study, in which the slow fluctuations in the charge channel and fast fluctuations in the spin channel compete on an equal footing.

The same general features as in the left panel of Fig. 6 are found in YBCO.[55] There is a narrow dispersionless peak at lowest binding energy, and a broader 'hump' at about 0.1 eV dispersing towards it. This is encouraging for our interpretation, since the antiadiabatic mechanism is quite generic, and one naturally expects all high-T_c superconductors to be in a broadly similar physical regime.

We have begun testing the same ideas in the electron-doped cuprates, and the first results reported here indicate one important difference from the hole-doped ones: the magnetic perturbation is lower in energy than the superconducting transition, so that 20 K is high temperature in NCCO, while 90 K is low in BSCCO. This fits well with the observed[13,14] coexistence of antiferromagnetic correlations with superconductivity in NCCO, with a characteristic scale of the former at 10 K, roughly half of T_c. At the same time, an interesting similarity has emerged, namely the oxygen degree of freedom seems to play an equally important role in both electron and hole compounds. These are both qualitative points and are not expected to be modified by further refinement. The first accounts for hot spot effects observed in NCCO, the second for the shape of the Fermi surface, which cuts the skew-diagonal of the zone where the Fermi surface dominated by copper-oxygen hopping would be expected to run parallel to it.

Superconductivity has not been explicitly included in our calculation. We have nevertheless accounted for all the main features of the ARPES data in BSCCO near the vH point, by a phenomenological treatment of the observed magnetic response below T_c. The superconducting scale of $\sim$100 K thus appears well isolated from the phenomena responsible for the ARPES profile, so we believe that taking it eventually into account will not invalidate our present results.

ACKNOWLEDGMENTS

Conversations with J. Friedel and E. Tutiš are gratefully acknowledged. This work was supported by the Croatian Government under Project 0119256.

REFERENCES

1. Z. X. Shen, W. E. Spicer, D. M. King, D. S. Dessau, and B. O. Wells, "Photoemission studies of high-T_c superconductors: the superconducting gap," *Science* **267**, pp. 343–50, 1995.
2. C. Kim, P. J. White, Z. X. Shen, T. Tohyama, Y. Shibata, S. Maekawa, B. O. Wells, Y. J. Kim, R. J. Birgeneau, and M. A. Kastner, "Systematics of the photoemission spectral function of cuprates: insulators and hole- and electron-doped superconductors," *Phys. Rev. Lett.* **80**, pp. 4245–8, 1998.
3. A. V. Fedorov, T. Valla, P. D. Johnson, Q. Li, G. D. Gu, and N. Koshizuka, "Temperature dependent photoemission studies of optimally doped $Bi_2Sr_2CaCu_2O_8$," *Phys. Rev. Lett.* **82**, pp. 2179–82, 1999.
4. T. Valla, A. V. Fedorov, P. D. Johnson, B. O. Wells, S. L. Hulbert, Q. Li, G. D. Gu, and N. Koshizuka, "Evidence for quantum critical behavior in the optimally doped cuprate $Bi_2Sr_2CaCu_2O_{8+\delta}$," *Science* **285**, pp. 2110–3, 1999.
5. H. M. Fretwell, A. Kaminski, J. Mesot, J. C. Campuzano, M. R. Norman, M. Randeria, T. S. R. Gatt, T. Takahashi, and K. Kadowaki, "Fermi surface of $Bi_2Sr_2CaCu_2O_8$," *Phys. Rev. Lett.* **84**, pp. 4449–52, 2000.
6. D. L. Feng, N. P. Armitage, D. H. Lu, A. Damascelli, J. P. Hu, P. Bogdanov, A. Lanzara, F. Ronning, K. M. Shen, H. Eisaki, C. Kim, and Z.-X. Shen, "Bilayer splitting in the electronic structure of heavily overdoped $Bi_2Sr_2CaCu_2O_{8+\delta}$," *Phys. Rev. Lett.* **86**, pp. 5550–3, 2001.

7. A. Kaminski, M. Randeria, J. C. Campuzano, M. R. Norman, H. Fretwell, J. Mesot, T. Sato, T. Takahashi, and K. Kadowaki, "Renormalization of spectral line shape and dispersion below T_c in $Bi_2Sr_2CaCu_2O_{8+\delta}$," *Phys. Rev. Lett.* **86**, pp. 1070–3, 2001.
8. J. Mesot, M. Randeria, M. R. Norman, A. Kaminski, H. M. Fretwell, J. C. Campuzano, H. Ding, T. Takeuchi, T. Sato, T. Yokoya, T. Takahashi, I. Chong, T. Terashima, M. Takano, T. Mochiku, and K. Kadowaki, "Determination of the fermi surface in high-T_c superconductors by angle-resolved photoemission spectroscopy," *Phys. Rev. B* **63**, p. 224516, 2001.
9. H. Matsui, T. Sato, T. Takahashi, S.-C. Wang, H.-B. Yang, H. Ding, T. Fujii, T. Watanabe, and A. Matsuda, "BCS-like Bogoliubov quasiparticle in high-T_c superconductors observed by angle-resolved photoemission spectroscopy," *Phys. Rev. Lett.* **90**, p. 217002, 2003.
10. J. C. Campuzano, M. R. Norman, and M. Randeria, "Photoemission in the high T_c superconductors," in *The Physics of Superconductors Vol. II: Novel Superconductors: Cuprate, Heavy-Fermion, and Organic Superconductors*, K. H. Bennemann and J. B. Ketterson, eds., Springer, 2004, to appear. cond-mat/0209476.
11. J. Rossat-Mignod, L. P. Regnault, C. Vettier, P. Burlet, J. Y. Henry, and G. Lapertot, "Investigation of the spin dynamics in $YBa_2Cu_3O_{6+x}$ by inelastic neutron scattering.," *Physica B* **169**, pp. 58–65, 1991.
12. K. Ishida, Y. Kitaoka, K. Asayama, K. Kadowaki, and T. Mochiku, "Spin correlations in the normal state of a $Bi_2Sr_2CaCu_2O_8$ single crystal," *Physica C* **263**, pp. 371–74, 1996.
13. K. Yamada, K. Kurahashi, Y. Endoh, R. J. Birgeneau, and G. Shirane, "Neutron scattering study on electron-hole doping symmetry of high-T_c superconductivity," *J. Phys. Chem. Solids* **60**, pp. 1025–30, 1999.
14. T. Uefuji, T. Kubo, K. Yamada, M. Fujita, K. Kurahashi, I. Watanabe, and K. Nagamine, "Coexistence of anti-ferromagnetic ordering and high-T_c superconductivity in electron-doped superconductor $Nd_{2-x}Ce_xCuO_4$," *Physica C* **357-360**, pp. 208–11, 2001.
15. Y. D. Chuang, A. D. Gromko, A. Fedorov, Y. Aiura, K. Oka, Y. Ando, H. Eisaki, S. I. Uchida, and D. S. Dessau, "Evidence for c-axis bilayer coupling," *Phys. Rev. Lett.* **87**, p. 117002, 2001.
16. A. A. Kordyuk, S. V. Borisenko, T. K. Kim, K. A. Nenkov, M. Knupfer, J. Fink, M. S. Golden, H. Berger, and R. Follath, "Origin of the peak-dip-hump line shape in the superconducting-state photoemission spectra of $Bi_2Sr_2CaCu_2O_8$," *Phys. Rev. Lett.* **89**, p. 077003, 2002.
17. A. Lanzara, P. V. Bogdanov, X. J. Zhou, S. A. Kellar, D. L. Feng, E. D. Lu, T. Yoshida, H. Eisaki, A. Fujimori, K. Kishio, J. I. Shimoyama, T. Noda, S. Uchida, Z. Hussain, and Z. X. Shen, "Evidence for ubiquitous strong electron-phonon coupling in high-temperature superconductors," *Nature* **412**, pp. 510–514, 2001.
18. T. Kiss, T. Yokoya, A. Chainani, and S. Shin, "Ultra-high resolution photoemission spectroscopy of simple metals: direct observation of superconducting gap and phonon-induced fine structures," *J. Electron Spectrosc. Relat. Phenom.* **114**, pp. 635–9, 2001.
19. T. Yokoya, A. Chainani, T. Kiss, S. Shin, K. Hirata, N. Kameda, T. Tamegai, T. Nishio, and H. Uwe, "High-resolution photoemission study of low-T_c superconductors: Phonon-induced electronic structures in low-T_c superconductors and comparison with the results of high-T_c cuprates," *Physica C* **378**, pp. 97–101, 2002.
20. D. M. Tang, J. Li, and C. D. Gong, "Role of the electron-phonon interaction in the d-wave superconductor," *Phys. Lett. A* **327**, pp. 344–51, 2004.
21. M. V. Sadovskii, "Pseudogap in high-T_c superconductors," *Uspekhi fizicheskih nauk* **171**, pp. 539–64, 2001.
22. S. A. Kivelson, I. P. Bindloss, E. Fradkin, V. Oganesyan, J. M. Tranquada, A. Kapitulnik, and C. Howald, "How to detect fluctuating stripes in the high-temperature superconductors," *Rev. Mod. Phys.* **75**, pp. 1201–41, 2003.
23. M. Eschrig and M. R. Norman, "Effect of the magnetic resonance on the electronic spectra of high-T_c superconductors," *Phys. Rev. B* **67**, pp. 144503/1–23, 2003.
24. Y. M. Vilk, "Shadow features and shadow bands in the paramagnetic state of cuprate superconductors," *Phys. Rev. B* **55**, pp. 3870–5, 1997.
25. P. W. Anderson, "The resonating valence bond state in La_2CuO_4 and superconductivity," *Science* **235**, p. 1196, 1987.
26. E. Dagotto, "Correlated electrons in high-temperature superconductors," *Rev. Mod. Phys.* **66**, p. 763, 1994.
27. G. Kotliar, P. A. Lee, and N. Read, "Fermi liquid description of $La_{2-x}Sr_xCuO_4$," *Physica C* **153-155**, pp. 538–42, 1988.
28. I. Mrkonjić and S. Barišić, "Singular behavior of the Emery model with O-O hopping for high-T_c superconductors," *Eur. Phys. J. B* **34**, pp. 69–84, 2003.

29. V. J. Emery, "Theory of high-T_c superconductivity in oxides," *Phys. Rev. Lett.* **58**, pp. 2794–7, 1987.
30. O. K. Andersenn, A. I. Liechtenstein, O. Jepsen, and F. Paulsen, "LDA energy bands, low-energy hamiltonians, t', t'', $t_\perp(k)$, and $J_\perp$," *J. Phys. Chem. Solids* **56**, pp. 1573–1591, 1995.
31. G. Aeppli, T. E. Mason, S. M. Hayden, H. A. Mook, and J. Kulda, "Nearly singular magnetic fluctuations in the normal state of a high-T_c cuprate superconductor," *Science* **278**, pp. 1432–5, 1997.
32. M. Kastner, R. Birgenau, G. Shirane, and Y. Endoh, "Magnetic, transport, and optical properties of monolayer copper oxides," *Rev. Mod. Phys.* **70**, pp. 897–928, 1998.
33. H. F. Fong, B. Keimer, D. Reznik, D. L. Milius, and I. A. Aksay, "Polarized and unpolarized neutron-scattering study of the dynamical spin susceptibility of $YBa_2Cu_3O_7$," *Phys. Rev. B* **54**, pp. 6708–20, 1996.
34. H. F. Fong, P. Bourges, Y. Sidis, L. P. Regnault, A. Ivanov, G. D. Gu, N. Koshizuka, and B. Keimer, "Neutron scattering from magnetic excitations in $Bi_2Sr_2CaCu_2O_{8+\delta}$," *Nature* **398**, pp. 588–91, 1999.
35. P. Bourges, Y. Sidis, H. F. Fong, L. P. Regnault, J. Bossy, A. Ivanov, and B. Keimer, "The spin excitation spectrum in superconducting $YBa_2Cu_3O_{6.85}$," *Science* **288**, pp. 1234–7, 2000.
36. J. Mesot, N. Metoki, M. Böhm, A. Hiess, and K. Kadowaki, "The magnetic resonance in underdoped Bi2212 and its relation to the electronic spectra: an inelastic neutron scattering study," *Physica C* **341-348**, pp. 2105–6, 2000.
37. H. He, Y. Sidis, P. Bourges, G. D. Gu, A. Ivanov, N. Koshizuka, B. Liang, C. T. Lin, L. P. Regnault, E. Schoenherr, and B. Keimer, "Resonant spin excitation in an overdoped high temperature superconductor," *Phys. Rev. Lett.* **86**, pp. 1610–3, 2001.
38. H. He, P. Bourges, Y. Sidis, C. Ulrich, L. P. Regnault, S. Pailhes, N. S. Berzigiarova, N. N. Kolesnikov, and B. Keimer, "Resonant spin excitation in an overdoped high temperature superconductor," *Science* **295**, p. 1045, 2002.
39. V. Hinkov, S. Pailhes, P. Bourges, Y. Sidis, A. Ivanov, A. Kulakov, C. T. Lin, D. P. Chen, C. Bernhard, and B. Keimer, "Two-dimensional geometry of spin excitations in the high-transition-temperature superconductor $YBa_2Cu_3O_{6+x}$," *Nature* **430**, pp. 650–3, 2004.
40. D. K. Morr, "The resonance peak in the high-T_c cuprates," *Physica B* **280**, pp. 178–179, 2000.
41. Y. M. Vilk and A. S. Tremblay, "Non-perturbative many-body approach to the Hubbard model and single-particle pseudogap," *J. Phys. I France* **7**, pp. 1309–68, 1997.
42. Y. Yanase, "Pseudogap and superconducting fluctuation in high-T_c cuprates: Theory beyond 1-loop approximation," *J. Phys. Soc. Jpn.* **73**, pp. 1000–17, 2004.
43. A. A. Abrikosov, L. P. Gorkov, and I. E. Dzaloshinski, *Methods of Quantum Field Theory in Statistical Physics*, Dover, 1975.
44. T. Valla, A. V. Fedorov, P. D. Johnson, Q. Li, G. D. Gu, and N. Koshizuka, "Temperature dependent scattering rates at the Fermi surface of optimally doped $Bi_2Sr_2CaCu_2O_{8+\delta}$," *Phys. Rev. Lett.* **85**, pp. 828–31, 2000.
45. M. R. Norman, M. Randeria, H. Ding, and J. C. Campuzano, "Phenomenological models for the gap anisotropy of BSCCO as measured by angle-resolved photoemission spectroscopy," *Phys. Rev. B* **52**, pp. 615–22, 1995.
46. Y. Yanase and K. Yamada, "Theory of transport phenomena in high-T_c cuprates," *J. Phys. Soc. Jpn.* **68**, pp. 548–60, 1999.
47. J. C. Campuzano, H. Ding, M. R. Norman, H. M. Fretwell, M. Randeria, A. Kaminski, J. Mesot, T. Takeuchi, T. Sato, T. Yokoya, T. Takahashi, T. Mochiku, K. Kadowaki, P. Guptasarma, D. G. Hinks, Z. Konstantinovic, Z. Z. Li, and H. Raffy, "Electronic spectra and their relation to the π, π collective mode in high-T_c superconductors," *Phys. Rev. Lett.* **83**, pp. 3709–2, 1999.
48. D. K. Sunko, "Fermion kinetics in the Falicov-Kimball limit of the three-band Emery model," *Eur. Phys. J. B* **43**, pp. 319–31, 2005.
49. N. P. Armitage, D. H. Lu, D. L. Feng, C. Kim, A. Damascelli, K. M. Shen, F. Ronning, and Z. Shen, "Superconducting gap anisotropy in $Nd_{1.85}Ce_{0.15}CuO_4$: Results from photoemission," *Phys. Rev. Lett.* **86**, pp. 1126–9, 2001.
50. Y. Onose, Y. Taguchi, K. Ishizaka, and Y. Tokura, "Doping dependence of pseudogap and related charge dynamics in $Nd_{2-x}Ce_xCuO_4$," *Phys. Rev. Lett.* **87**, pp. 217001–1/4, 2001.
51. N. P. Armitage, D. H. Lu, C. Kim, A. Damascelli, K. M. Shen, F. Ronning, D. L. Feng, P. Bogdanov, and Z. Shen, "Anomalous electronic structure and pseudogap effects in $Nd_{1.85}Ce_{0.15}CuO_4$," *Phys. Rev. Lett.* **87**, pp. 147003–1/4, 2001.
52. T. Sato, T. Kamiyama, T. Takahashi, K. Kurahashi, and K. Yamada, "Observation of $d_{x^2-y^2}$-like superconducting gap in an electron-doped high-temperature superconductor," *Nature* **291**, pp. 1517–19, 2001.

53. N. P. Armitage, F. Ronning, D. H. Lu, C. Kim, A. Damascelli, K. M. Shen, D. L. Feng, H. Eisaki, and Z. Shen, "Doping dependence of an n-type cuprate superconductor investigated by angle-resolved photoemission spectroscopy," *Phys. Rev. Lett.* **88**, pp. 257001–1/4, 2002.
54. G. Blumberg, A. Koitzsch, A. Gozar, B. S. Dennis, C. A. Kendziora, P. Fournier, and R. L. Greene, "Nonmonotonic $d_{x^2-y^2}$ superconducting order parameter in $Nd_{2-x}Ce_xCuO_4$," *Phys. Rev. Lett.* **88**, pp. 107002–1/4, 2002.
55. D. H. Lu, D. L. Feng, N. P. Armitage, K. M. Shen, A. Damascelli, C. Kim, F. Ronning, and Z.-X. Shen, "Superconducting gap and strong in-plane anisotropy in untwinned $YBa_2Cu_3O_{7-\delta}$," *Phys. Rev. Lett.* **86**, pp. 4370–3, 2001.